Factor Graph-based Multipath-assisted Indoor Passive Localization with Inaccurate Receiver

Ganlin Hao, Nan Wu, Yifeng Xiong, Hua Wang and Jingming Kuang
School of Information and Electronics, Beijing Institute of Technology,
Beijing, 100081 - China
[e-mail: wunan@bit.edu.cn]
*Corresponding author: Nan Wu

Received September 17, 2015; revised December 3, 2015; accepted December 22, 2015; published February 29, 2016

Abstract

Passive wireless devices have increasing civilian and military applications, especially in the scenario with wearable devices and Internet of Things. In this paper, we study indoor localization of a target equipped with radio-frequency identification (RFID) device in ultra-wideband (UWB) wireless networks. With known room layout, deterministic multipath components, including the line-of-sight (LOS) signal and the reflected signals via multipath propagation, are employed to locate the target with one transmitter and a single inaccurate receiver. A factor graph corresponding to the joint posterior position distribution of target and receiver is constructed. However, due to the mixed distribution in the factor node of likelihood function, the expressions of messages are intractable by directly applying belief propagation on factor graph. To this end, we approximate the messages by Gaussian distribution via minimizing the Kullback-Leibler divergence (KLD) between them. Accordingly, a parametric message passing algorithm for indoor passive localization is derived, in which only the means and variances of Gaussian distributions have to be updated. Performance of the proposed algorithm and the impact of critical parameters are evaluated by Monte Carlo simulations, which demonstrate the superior performance in localization accuracy and the robustness to the statistics of multipath channels.

Keywords: Passive Localization, Multipath, Inaccurate Receiver, Factor Graph, Belief Propagation

This work is supported by "National Science Foundation of China (NSFC)" (Grant Nos. 61201181, 61471037) and "A Foundation for the Author of National Excellent Doctoral Dissertation of P. R. China (FANEDD)" (Grant No.201445).

http://dx.doi.org/10.3837/tiis.2016.02.015 **ISSN : 1976-7277**

1. Introduction

Context-awareness has attracted enormous interest in wireless networks. This trendency motivates the demand for precise localization. Indoor passive localization awareness plays a crucial role in many fields such as life-saving, asset tracking, environmental monitoring and privacy security [1-3]. However, locating the target in indoor multipath environment is still quite challenging. Fortunately, owing to the fine time-resolution, Ultra-wideband (UWB) signals are potential candidates for localization in harsh multipath environments [4].

Localization based on time-of-arrival (TOA) have been widely investigated. Many existing algorithms utilize the line-of-sight (LOS) signal only, which leads to positioning error in non-line-of-sight (NLOS) environment. Generally speaking, NLOS mitigation techniques can be used to reduce the impact on location accuracy [5]. However, NLOS signals, e.g., strong single reflections, contain useful information which may benefit the passive localization. The reflections signals named deterministic multipath components (MPCs) coming from walls can be used to extract additional position information and realize the multipath assisted localization with the concept of *virtual anchors* (VAs). With the help of VAs, it is possible to reduce the number of transmitters and receivers to obtain high localization accuracy.

Different from the active localization, to use the deterministic MPCs between the target and the receiver, Time-reversal (TR) processing [6] has been used in backscatter channels [7], which can insure the signals coming from the transmitter arrive to the target at the same TOA by calibrating the delay parameters of signals. According to the energy focused on the target by TR processing, the passive targets scatter the signals using passive transponder, e.g., radio-frequency identification (RFID) tag. After that, the RFID modulated signals received by the receiver can be distinguished from other multipath signals at the receiver side [8]. However, to the best knowledge of the authors, multipath-assisted algorithms in passive localization scenario has not been studied. Moreover, all the above passive localization researches assume that the receivers' locations are perfectly known. In practice, however, utilizing the inaccurate position information of the receiver will lead to positioning error.

The contributions of this paper can be summarized as follows:

We propose a factor graph-based [9] algorithm which can locate the target by one transmitter and a single inaccurate receiver in multipath indoor scenario. For messages on factor graph which are difficult to be expressed and updated, Kullback-Leibler divergence (KLD) minimization is employed to obtain a low complexity parametric message passing algorithm. Simulation results show that the proposed algorithm outperforms the particle-based algorithm and approximated maximum a posteriori probability (AMAP) algorithm.

The rest of this paper is organized as follows. The system model is given in Section 2. In Section 3, factor graph is constructed and the proposed parametric message passing algorithm is derived. The performance of the proposed algorithm and the impact of critical parameters are evaluated in Section 4. Finally, the conclusions are drawn in Section 5.

2. Related Work

Using UWB signals in passive localization, a TOA based two-step estimation (TSE) algorithm is proposed for passive localization in [10]. Passive localization in quasi-synchronous network is investigated in [11]. In [8], a novel network architecture which jointly localizes passive tags and moving passive objects through the discrimination of their backscattered responses is studied. Different from the above algorithms with LOS signals, it is shown in [12] that deterministic multipath components (MPCs) can be used to extract additional position information and realize the multipath assisted localization with the concept of VAs. In [13], position error bound based on the equivalent Fisher information matrix (EFIM) in indoor passive localization is derived, which obtained a lower bound with the help of TR process. However, in this scenario, multipath-assisted algorithm in passive localization scenario has not been considered. Moreover, the receiver's position uncertainty is not taking into account.

3. System Model

We consider a passive indoor localization scenario illustrated in **Fig. 1**, which consists of a transmitter, a receiver and a target. For simplicity, we assume a perfect synchronous circumstance and the floorplan is known. At the beginning, the transmitter generates signal $s(t)$ based on the TR processing, which is composed of an assembly of complex weighted gain and time delay components of pulse $p(t)$.

$$s(t) = [\sum_{k=1}^{N_{\mathrm{TX}}} \hat{a}_{k,\mathrm{TX}}^{*} \delta(t + \hat{\tau}_{k,\mathrm{TX}} - \hat{\tau}_{1,\mathrm{TX}})] * p(t) \tag{1}$$

where $\hat{a}_{k,TX}^{*}$ expresses the complex weight determined, $\hat{\tau}_{k,\mathrm{TX}}$ denotes the corresponding delay of each $\mathrm{VA}_{\mathrm{TX}}$, and $\hat{\tau}_{1,\mathrm{TX}}$ is the transmission delay of the LOS signal. TR processing has the intrinsic attributes to overcome the degeneration of pinhole channels caused by multipath propagation in indoor scenario, because it concentrates the radiant energy onto the target [7] after the LOS propagation's time between the transmitter and the target.

We assume that the MPC parameters between the transmitter and the target used in TR process in (1) are perfectly estimated [13]. Then the signal is modulated by commercial passive ultra-high frequency (UHF) RFID tag in target. At the receiver side, signal can be distinguished from other multipath signals (clutters) [8].

Let's assume the transmitter's position is $\phi \triangleq [0\ 0]^T$ and the target's position is $\boldsymbol{\varphi} \triangleq [x_\varphi\ y_\varphi]^T$. In a time slot, the transmitter sends signal $s(t)$. Then the scattered signals after RFID modulation transmitted to the receiver consists of LOS signal and reflected signals. As TR processing calibrates the delay parameters of signals among the single reflections between the transmitter's VAs and the target, the delay equals the LOS measurement between the transmitter and target. With the use of floorplan information, single reflections can be interpreted as LOS signals between the target and $\mathrm{VA}_{\mathrm{RX},i}$ in **Fig. 1**, which is useful for localization. Now we get a series of measurements from the transmitter to the receiver (or $\mathrm{VA}_{\mathrm{RX},i}$) via the target.

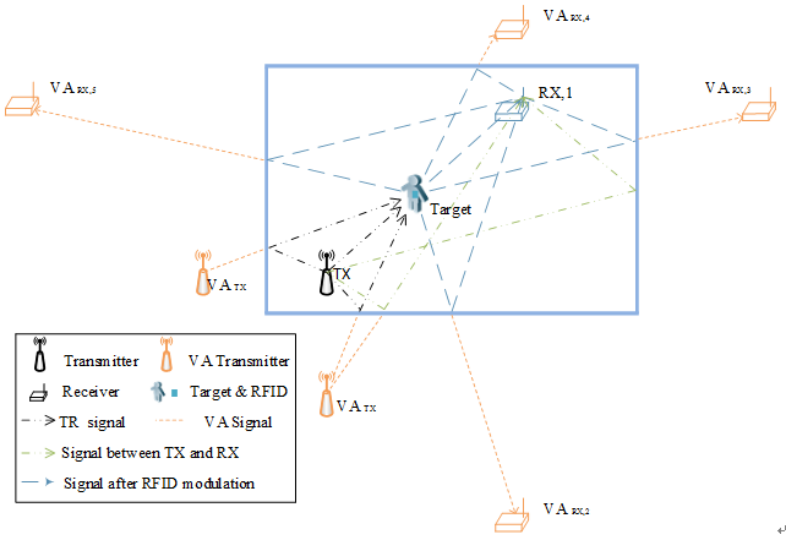

Fig. 1. Floorplan with a transmitter (TX) node, receiver (RX) node and a subset of Virtual Receivers (i.e. $\mathrm{VA}_{\mathrm{RX},i}$, $i \in 2,3,4,5$).

The position of the receiver is $\boldsymbol{\theta}_1 \triangleq [x_{\theta_1}\ y_{\theta_1}]^T$ and that of the virtual receiver $\mathrm{VA}_{\mathrm{RX},i}$ is $\boldsymbol{\theta}_i \triangleq [x_{\theta_i}\ y_{\theta_i}]^T, i = 2,...,N_{\mathrm{RX}}$, which are stacked to the vector $\boldsymbol{\theta} \triangleq \left[\boldsymbol{\theta}_1^T\ \boldsymbol{\theta}_2^T \cdots \boldsymbol{\theta}_{N_{\mathrm{RX}}}^T\right]^T$. Since we only consider the LOS component and the single reflections between the target and the receiver as deterministic MPCs, the maximum number of deterministic components in MPCs is $N_{\mathrm{RX}} = 5$. We assume the deterministic MPCs are orthogonal, which means no overlapping and are convenient to detection. After detection, multiplying Δt_m by the signal propagation speed c, the range measurements from transmitter to receiver and virtual receiver via target can be expressed as

$$R_m = c \cdot \Delta t_m + n_{R_m} = \sqrt{x_\varphi^2 + y_\varphi^2} + \sqrt{(x_\varphi - x_{\theta_m})^2 + (y_\varphi - y_{\theta_m})^2} + n_{R_m},\quad m = 1,...,N_{\mathrm{RX}} \tag{2}$$

where Δt_m is signal propagation time, R_m is the range measurement from the *m*-th multipath, n_{R_m} is the range measurement noise, which is zero-mean Gaussian distributed with variance $\sigma_{R_m}^2$, i.e., $n_{R_m} \sim N(0, \sigma_{R_m}^2)$.

Since the deterministic MPCs may be sheltered by obstacles and the clutters may exist in indoor scenario, we cannot associate each ranging measurement $\{R_m\}$ with each $\mathrm{VA}_{\mathrm{RX}}$ accurately. Therefore, a probatilistic approach is an appropriate alternative, where each measurement is received by a certain virtual receiver with probability. Accordingly, the likelihood function $p(R_m \mid \boldsymbol{\theta}, \boldsymbol{\varphi})$ can be expressed as

$$p(R_m \mid \boldsymbol{\theta}, \boldsymbol{\varphi}) = \frac{(1 - P_{\mathrm{VA}})}{R_{\max}} + \frac{P_{\mathrm{VA}}}{P_{\mathrm{v}}} \sum_{j=1}^{N_{\mathrm{RX}}} P_{\mathrm{v},j} N(R_m; \| \boldsymbol{\theta}_j - \boldsymbol{\varphi} \| + \| \phi - \boldsymbol{\varphi} \|, \sigma_{R_m}^2) \tag{3}$$

where P_{VA} is the probability that R_m belongs to deterministic MPCs, $P_{\mathrm{v},p} / P_{\mathrm{v}}$ is the probability that R_m is the *m*-th multipath component, normalization factor $P_{\mathrm{v}} = \sum_{j}^{N_{\mathrm{RX}}} P_{\mathrm{v},j}$. The

former part in (3) denotes that R_m is clutter with probability $(1-P_{\mathrm{VA}})$, which is uniformly distributed over the range from zero to a maximum ranging value $R_{\max}$.

Based on the assumption that the range measurements in deterministic MPCs are independent, the joint likelihood distribution $p(\mathbf{R}\,|\,\boldsymbol{\theta},\boldsymbol{\varphi})$ is given by

$$p(\mathbf{R}\,|\,\boldsymbol{\theta},\boldsymbol{\varphi}) = \prod_{m=1}^{N_{\mathrm{RX}}} p(R_m\,|\,\boldsymbol{\theta},\boldsymbol{\varphi}) \tag{4}$$

where $\mathbf{R} \triangleq \left[R_1\ R_2 \cdots R_{N_{\mathrm{RX}}} \right]^T$.

Besides the above range measurements $\mathbf{R}$, the receiver can also obtain the range measurements from transmitter to receiver (or virtual receiver $\mathrm{VA}_{\mathrm{RX},i}$), which are expressed as

$$D_i = c\cdot\Delta\tau_i + n_{D_i} = \sqrt{x_{\theta_i}{}^2 + y_{\theta_i}{}^2} + n_{D_i},\quad i=1,\ldots,N_{\mathrm{RX}} \tag{5}$$

where $\Delta\tau_i$ is signal propagation time between $\boldsymbol{\phi}$ and $\boldsymbol{\theta}_i$, $n_{D_i} \sim N(0,\sigma_{D_i}^2)$. As we assume the receiver has a minor ambiguity in indoor scenario, it is possible to associate D_i with each receiver and virtual receiver $\mathrm{VA}_{\mathrm{RX},i}$ according to the Euclidean distance constraint.

Accordingly, the joint likelihood function of the range measurement between $\boldsymbol{\varphi}$ and $\boldsymbol{\theta}_i$ are given by

$$p(\mathbf{D}\,|\,\boldsymbol{\theta}) = \prod_{i=1}^{N_{\mathrm{RX}}} p(D_i\,|\,\boldsymbol{\theta}_i) \tag{6}$$

where $\mathbf{D} \triangleq [D_1\ D_2 \cdots D_{N_{\mathrm{RX}}}]^T$ and $p(D_i\,|\,\boldsymbol{\theta}_i)$ is

$$p(D_i\,|\,\boldsymbol{\theta}_i) = N(D_i; \|\,\boldsymbol{\theta}_i - \boldsymbol{\phi}\,\|, \sigma_{D_i}^2) \tag{7}$$

4. Message Passing Algorithm for Passive Localization

Since the range measurements $\mathbf{R}$ and $\mathbf{D}$ are independent, the joint posterior distribution of positions of the target and receiver can be expressed as

$$p(\boldsymbol{\varphi},\boldsymbol{\theta}\,|\,\mathbf{R},\mathbf{D}) = p(\boldsymbol{\varphi},\boldsymbol{\theta}\,|\,\mathbf{R})\,p(\boldsymbol{\theta}\,|\,\mathbf{D}) \tag{8}$$

Using the Bayes' rule, we have

$$p(\boldsymbol{\varphi},\boldsymbol{\theta}\,|\,\mathbf{R}) \propto p(\mathbf{R}\,|\,\boldsymbol{\varphi},\boldsymbol{\theta})\,p(\boldsymbol{\theta})\,p(\boldsymbol{\varphi}) = \prod_{m=1}^{N_{\mathrm{RX}}} \left(p(R_m\,|\,\boldsymbol{\theta},\boldsymbol{\varphi}) \prod_{i=1}^{N_{RX}} p(\boldsymbol{\theta}_i) \right) p(\boldsymbol{\varphi}) \tag{9}$$

$$p(\boldsymbol{\theta}\,|\,\mathbf{D}) \propto p(\mathbf{D}\,|\,\boldsymbol{\theta})\,p(\boldsymbol{\theta}) = \prod_{i=1}^{N_{\mathrm{RX}}} p(D_i\,|\,\boldsymbol{\theta}_i)\,p(\boldsymbol{\theta}_i) \tag{10}$$

where $p(\boldsymbol{\theta}_i) = \int p(\boldsymbol{\theta}_i\,|\,\boldsymbol{\theta}_1)\,p(\boldsymbol{\theta}_1)\,d\boldsymbol{\theta}_1$ for $i \in \{2,3,4,5\}$.

The corresponding posterior distributions for the target and the receiver can be calculated by marginalizing the joint distribution in (9) and (10), i.e.

$$p(\boldsymbol{\varphi}\,|\,\mathbf{R},\mathbf{D}) \propto \int p(\boldsymbol{\varphi},\boldsymbol{\theta}\,|\,\mathbf{R})\,p(\boldsymbol{\theta}\,|\,\mathbf{D})\,d\boldsymbol{\theta} \tag{11}$$

$$p(\boldsymbol{\theta}_1 \mid \mathbf{R},\mathbf{D}) \propto \iint p(\boldsymbol{\varphi},\boldsymbol{\theta} \mid \mathbf{R})\, p(\boldsymbol{\theta} \mid \mathbf{D})\, d\boldsymbol{\varphi} d\boldsymbol{\theta} \setminus \boldsymbol{\theta}_1 \tag{12}$$

where '$\boldsymbol{\theta} \setminus \boldsymbol{\theta}_1$' denotes the variables in $\boldsymbol{\theta}$ except $\boldsymbol{\theta}_1$.The marginalization in (11) and (12) can be efficiently calculated by message passing algorithm on factor graph. Using the factorization in (9) and (10), factor graph of the joint posterior distribution in (8) is illustrated in **Fig. 2**. It is seen that the factor graph contains cycles, which leads to iterative message passing algorithm.

The factor nodes $G(\boldsymbol{\theta},\boldsymbol{\varphi})$ and $H(\boldsymbol{\theta})$ denote the joint likelihood functions $p(\mathbf{R} \mid \boldsymbol{\theta},\boldsymbol{\varphi})$ and $p(\mathbf{D} \mid \boldsymbol{\theta})$, respectively, which can be further factorized to $G(\boldsymbol{\theta},\boldsymbol{\varphi}) = \prod_{i=1}^{N_{\mathrm{RX}}} g_{R_m}(\boldsymbol{\theta},\boldsymbol{\varphi})$, $p(\mathbf{D} \mid \boldsymbol{\theta}) = \prod_{i=1}^{N_{\mathrm{RX}}} h_{D_i}(\boldsymbol{\theta}_i)$ with $g_{R_m}(\boldsymbol{\theta},\boldsymbol{\varphi}) = p(R_m \mid \boldsymbol{\theta},\boldsymbol{\varphi})$ and $h_{D_i}(\boldsymbol{\theta}_i) = p(D_i \mid \boldsymbol{\theta}_i)$. The prior position distributions of target $\boldsymbol{\varphi} \triangleq [x_\varphi \; y_\varphi]^T$ and receiver $\boldsymbol{\theta}_1 \triangleq [x_{\theta_1} \; y_{\theta_1}]^T$ are assumed to be

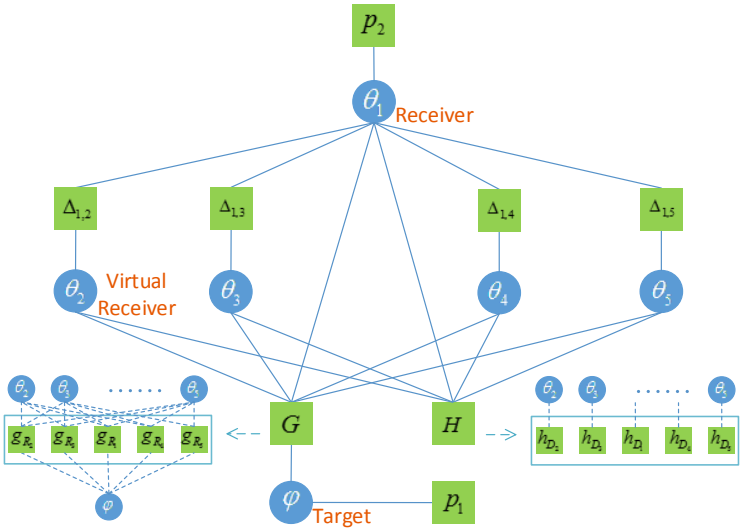

Fig. 2. Factor Graph for the passive localization network.

Gaussian distributions, i.e.

$$p_1(\boldsymbol{\varphi}) = p(\boldsymbol{\varphi}) = \frac{1}{2\pi(\sigma_{\boldsymbol{\varphi}}^{(0)})^2} \exp\left(-\frac{\| \boldsymbol{\varphi} - \bar{\boldsymbol{\varphi}} \|^2}{2(\sigma_{\boldsymbol{\varphi}}^{(0)})^2} \right) \tag{13}$$

$$p_2(\boldsymbol{\theta}_1) = p(\boldsymbol{\theta}_1) = \frac{1}{2\pi(\sigma_{\boldsymbol{\theta}_1}^{(0)})^2} \exp\left(-\frac{\| \boldsymbol{\theta}_1 - \bar{\boldsymbol{\theta}}_1 \|^2}{2(\sigma_{\boldsymbol{\theta}_1}^{(0)})^2} \right) \tag{14}$$

where $\bar{\boldsymbol{\varphi}}$ and $\bar{\boldsymbol{\theta}}_1$ are the true positions of the target and receiver, respectively, $(\sigma_{\boldsymbol{\varphi}}^{(0)})^2$ and $(\sigma_{\boldsymbol{\theta}_1}^{(0)})^2$ represent position uncertainties. Assuming x-axis and y-axis of the position coordinates are independent, with $(\sigma_{\boldsymbol{\varphi}}^{(0)})^2 = (\sigma_{x_\varphi}^{(0)})^2 = (\sigma_{y_\varphi}^{(0)})^2$, $(\sigma_{\boldsymbol{\theta}_1}^{(0)})^2 = (\sigma_{x_{\theta_1}}^{(0)})^2 = (\sigma_{y_{\theta_1}}^{(0)})^2$.

Since $\mathrm{VA}_{\mathrm{RX},i}, i \in \{2,...,N_{\mathrm{RX}}\}$ is the symmetrical mirror image of the receiver, we use the indicator function $\Delta_{1,i}(\boldsymbol{\theta}_1,\boldsymbol{\theta}_i), i \in \{2,...,N_{\mathrm{RX}}\}$ to represent position constraints between $\boldsymbol{\theta}_1$ and

$\boldsymbol{\theta}_i$. Therefore, $p(\boldsymbol{\theta}_i \mid \boldsymbol{\theta}_1) = \Delta_{1,i}(\boldsymbol{\theta}_1, \boldsymbol{\theta}_i)$ can be expressed as

$$\Delta_{1,i}(x_{\theta_1}, x_{\theta_i}) \triangleq \begin{cases} \delta(x_{\theta_1} - x_{\theta_i}) & i = 2 \quad or \quad 4 \\ \delta(x_{\theta_1} + x_{\theta_i}) & i = 5 \\ \delta(x_{\theta_1} + x_{\theta_i} - 2L) & i = 3 \end{cases} \tag{15}$$

$$\Delta_{1,i}(y_{\theta_1}, y_{\theta_i}) \triangleq \begin{cases} \delta(y_{\theta_1} - y_{\theta_i}) & i = 3 \quad or \quad 5 \\ \delta(y_{\theta_1} + y_{\theta_i}) & i = 2 \\ \delta(y_{\theta_1} + y_{\theta_i} - 2W) & i = 4 \end{cases} \tag{16}$$

where $\mathrm{L} \times \mathrm{W}$ describe the dimensions in this room and each virtual receiver $\mathrm{VA}_{\mathrm{RX},i}$ has the same position uncertainty $(\sigma_{\boldsymbol{\theta}_1}^{(0)})^2$. In fact, the variables are the target and receiver's positions only, which means the mirror variables $\boldsymbol{\theta}_i, i \in \{2,...,N_{\mathrm{RX}}\}$, can be decided by (15) and (16). Nevertheless, we draw the mirror variables $\boldsymbol{\theta}_i$ on factor graph to ease the derivation.

Then we calculate the corresponding messages on factor graph from the top to the bottom. Firstly, the messages from $\boldsymbol{\theta}_1$ to $\Delta_{1,i}$ are given by

$$\mu_{\boldsymbol{\theta}_1 \to \Delta_{1,i}}^{(l-1)}(\boldsymbol{\theta}_1) = \frac{1}{2\pi(\sigma_{\boldsymbol{\theta}_1}^{(0)})^2} \exp\left(-\frac{\| \boldsymbol{\theta}_1 - \bar{\boldsymbol{\theta}}_1 \|^2}{2(\sigma_{\boldsymbol{\theta}_1}^{(0)})^2} \right) \tag{17}$$

where $\boldsymbol{\theta}_1 = (x_{\theta_1}, y_{\theta_1})$.

Secondly, the messages from $\Delta_{1,i}$ to $\boldsymbol{\theta}_i, i \in \{2,3,4,5\}$ are given by

$$\mu_{\Delta_{1,i} \to \boldsymbol{\theta}_i}^{(l)}(x_{\theta_i}) \propto \int \Delta_{1,i}(x_{\theta_1}, x_{\theta_i}) \mu_{\boldsymbol{\theta}_1 \to \Delta_{1,i}}^{(l-1)}(x_{\theta_1}) dx_{\boldsymbol{\theta}_1} \tag{18}$$

$$\mu_{\Delta_{1,i} \to \boldsymbol{\theta}_i}^{(l)}(y_{\theta_i}) \propto \int \Delta_{1,i}(y_{\theta_1}, y_{\theta_i}) \mu_{\boldsymbol{\theta}_1 \to \Delta_{1,i}}^{(l-1)}(y_{\theta_1}) dy_{\boldsymbol{\theta}_1} \tag{19}$$

Based on $\mu_{\Delta_{1,i} \to \boldsymbol{\theta}_i}^{(l)}(\theta_i)$ obtained in (18)-(19), the messages from factor node $g_{R_m}(\boldsymbol{\theta}, \boldsymbol{\varphi})$ in $G(\boldsymbol{\theta}, \boldsymbol{\varphi})$ to variable nodes $\varphi=(x_\varphi, y_\varphi)$ are given by

$$\mu_{g_{R_m} \to \boldsymbol{\varphi}}^{(l)}(\boldsymbol{\varphi}) \propto \frac{(1 - P_{\mathrm{VA}})}{R_{\max}} + \frac{P_{\mathrm{VA}}}{P_{\mathrm{v}}} \sum_{j=1}^{N_{\mathrm{RX}}} P_{\mathrm{v},j} N(\boldsymbol{\varphi}; m_{g_{R_m}, \boldsymbol{\theta}_j \to \boldsymbol{\varphi}}^{(l)}, (\sigma_{g_{R_m}, \boldsymbol{\theta}_j \to \boldsymbol{\varphi}}^{(l)})^2) \tag{20}$$

The details of message passing algorithm on $\mu_{g_{R_m} \to \boldsymbol{\varphi}}^{(l)}(\boldsymbol{\varphi})$ are shown in Appendix A.

After having all the normalized messages to the variable $\boldsymbol{\varphi}$, the belief of target position can be calculated by multiplying all the incoming messages, i.e.

$$b_{\boldsymbol{\varphi}|\mathbf{R}}^{(l)}(\boldsymbol{\varphi}) = \prod_{m=1}^{N_{\mathrm{RX}}} \mu_{g_{R_m} \to \boldsymbol{\varphi}}^{(l)}(\boldsymbol{\varphi}) \mu_{p_1 \to \boldsymbol{\varphi}}^{(l)}(\boldsymbol{\varphi}) \tag{21}$$

Substituting (20) into (21), and taking into account the prior distribution given in (13), the beliefs $b_{\boldsymbol{\varphi}|\mathbf{R}}^{(l)}(\boldsymbol{\varphi})$ can be calculated, which are quite complex to be expressed and intractable to be used in the next iteration of message passing on factor graph.

As it is shown in **Fig. 3**(a), the multiplication $\prod_{m=1}^{N_{\mathrm{RX}}} \mu_{g_{R_m}\to\boldsymbol{\varphi}}(\boldsymbol{\varphi})$ in (21) has a series of local maxima, which may cause large positioning error. With the constraint of Gaussian prior distribution, the belief $b_{\boldsymbol{\varphi}|\mathbf{R}}^{(l)}(\boldsymbol{\varphi})$ is illustrated in **Fig. 3**(b). Note that since the prior is not accurate, $b_{\boldsymbol{\varphi}|\mathbf{R}}^{(l)}(\boldsymbol{\varphi})$ may still contain multiple local maxima. Nevertheless, the result in **Fig. 3**(b) is close to Gaussian distribution.

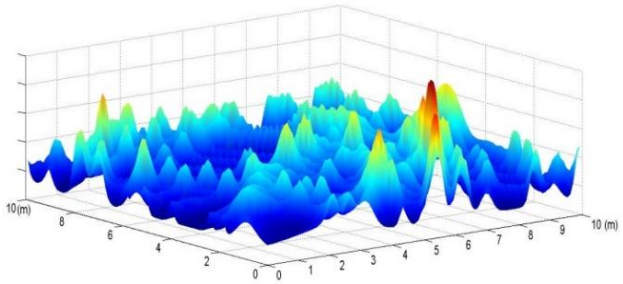

(a) Likelihood function

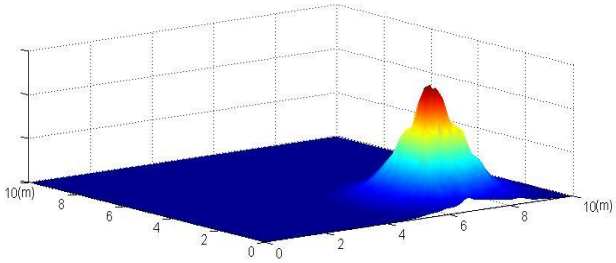

(b) The original belief $b_{\boldsymbol{\varphi}|\mathbf{R}}^{(l)}(\boldsymbol{\varphi})$

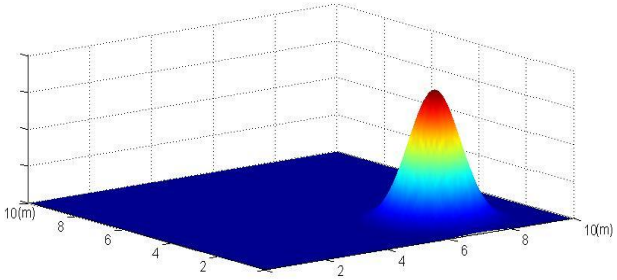

(c) Approximated belief $b_{\boldsymbol{\varphi}|\mathbf{R}}^{(l)*}(\boldsymbol{\varphi})$ via KLD minimization

Fig. 3. Illustration of the target's likelihood function, original belief $b_{\boldsymbol{\varphi}|\mathbf{R}}^{(l)}(\boldsymbol{\varphi})$ and the approximated belief $b_{\boldsymbol{\varphi}|\mathbf{R}}^{(l)*}(\boldsymbol{\varphi})$ via KLD minimization.

Based on this observation, we are able to approximate the belief of target position by a Gaussian distribution, i.e.,

$$b_{\boldsymbol{\varphi}}^{(l)}(\boldsymbol{\varphi}) = \frac{1}{2\pi\hat{\sigma}_{\boldsymbol{\varphi}}^2}\exp\left(-\frac{\|\boldsymbol{\varphi}-\tilde{\boldsymbol{\varphi}}\|^2}{2\hat{\sigma}_{\boldsymbol{\varphi}}^2}\right) \tag{22}$$

A general metric of closeness between two distributions is the Kullback-Leibler divergence (KLD) [14], which is given by

$$D(b_{\boldsymbol{\varphi}}^{(l)} \| b_{\boldsymbol{\varphi}|\mathbf{R}}^{(l)}) = \int b_{\boldsymbol{\varphi}}^{(l)}(\boldsymbol{\varphi}) ln \frac{b_{\boldsymbol{\varphi}}^{(l)}(\boldsymbol{\varphi})}{b_{\boldsymbol{\varphi}|\mathbf{R}}^{(l)}(\boldsymbol{\varphi})} d\boldsymbol{\varphi} \tag{23}$$

Substituting (21) and (22) into (23), yields

$D(b_{\boldsymbol{\varphi}}^{(l)} \| b_{\boldsymbol{\varphi}|\mathbf{R}}^{(l)}) =$

$$\int b_{\boldsymbol{\varphi}}^{(l)}(\boldsymbol{\varphi}) \ln b_{\boldsymbol{\varphi}}^{(l)}(\boldsymbol{\varphi}) d\boldsymbol{\varphi} - \int b_{\boldsymbol{\varphi}}^{(l)}(\boldsymbol{\varphi}) \ln \mu_{p_1 \to \boldsymbol{\varphi}}^{(l)}(\boldsymbol{\varphi}) d\boldsymbol{\varphi} - \int b_{\boldsymbol{\varphi}}^{(l)}(\boldsymbol{\varphi}) \ln \prod_{m=1}^{N_{\mathrm{RX}}} \mu_{g_{R_m} \to \boldsymbol{\varphi}}^{(l)}(\boldsymbol{\varphi}) d\boldsymbol{\varphi} \tag{24}$$

Then, the goal is to find $b_{\boldsymbol{\varphi}|\mathbf{R}}^{(l)*}$ in a given class R of Gaussian distribution to minimize the KLD

$$b_{\boldsymbol{\varphi}|\mathbf{R}}^{(l)*}(\boldsymbol{\varphi}) = \arg \min_{b_{\boldsymbol{\varphi}}^{(l)} \in R} D(b_{\boldsymbol{\varphi}}^{(l)} \| b_{\boldsymbol{\varphi}|\mathbf{R}}^{(l)}) \tag{25}$$

The minimization in (25) can be easily solved by numerical method. Then, the beliefs are approximated by Gaussian expression

$$b_{\boldsymbol{\varphi}|\mathbf{R}}^{(l)*}(\boldsymbol{\varphi}) \propto N(\boldsymbol{\varphi}; m_{\boldsymbol{\varphi}}^{(l)}, (\sigma_{\boldsymbol{\varphi}}^{(l)})^2) \tag{26}$$

which is drawn in **Fig. 3**(c).

Given the Gaussian approximation of the beliefs, the messages $\mu_{\boldsymbol{\varphi} \to g_{R_m}}^{(l)}(\boldsymbol{\varphi}), m \in \{1, ..., N_{\mathrm{RX}}\}$ are still intractable using the standard belief propagation rules. To this end, we resort to use the belief $b_{\boldsymbol{\varphi}|\mathbf{R}}^{(l)*}(\boldsymbol{\varphi})$ to approximate $\mu_{\boldsymbol{\varphi} \to R_m}^{(l)}(\boldsymbol{\varphi})$.

Then we will calculate the messages on the factor graph from the bottom to the top.

Firstly, the message from node g_{R_m} to $\boldsymbol{\theta}_i$ in factor G can be calculated by

$$\mu_{g_{R_m} \to \boldsymbol{\theta}_i}^{(l)}(\boldsymbol{\theta}_i) \propto \frac{(1 - P_{\mathrm{VA}})}{R_{\max}} + \frac{P_{\mathrm{VA}}}{P_{\mathrm{v}}} \sum_{j=1}^{N_{\mathrm{RX}}} P_{\mathrm{v},j} N(\boldsymbol{\theta}_i; m_{g_{R_m,j} \to \boldsymbol{\theta}_i}^{(l)}, (\sigma_{g_{R_m,j} \to \boldsymbol{\theta}_i}^{(l)})^2) \tag{27}$$

the message from node h_{D_i} to $\boldsymbol{\theta}_i$ in factor H can be calculated by

$$\mu_{h_{D_i} \to \boldsymbol{\theta}_i}^{(l)}(\boldsymbol{\theta}_i) \propto N\left(\boldsymbol{\theta}_i; m_{h_{D_i} \to \boldsymbol{\theta}_i}^{(l)}, (\sigma_{h_{D_i} \to \boldsymbol{\theta}_i}^{(l)})^2\right) \tag{28}$$

The details of message passing algorithm on $\mu_{g_{R_m} \to \boldsymbol{\theta}_i}^{(l)}(\boldsymbol{\theta}_i)$ and $\mu_{h_{D_i} \to \boldsymbol{\theta}_i}^{(l)}(\boldsymbol{\theta}_i)$ are shown in Appendix B.

Based on the indicator function $\Delta_{1,i}(\boldsymbol{\theta}_1, \boldsymbol{\theta}_i), i \in \{2, ..., N_{\mathrm{RX}}\}$, for coordinate x_{θ_i} in variable $\boldsymbol{\theta}_i$, $\mu_{g_{R_m} \to x_{\theta_i}}^{(l)}$ multiplies $\mu_{h_{D_i} \to x_{\theta_i}}^{(l)}$ turns to be the message from $\Delta_{1,i}$ to x_{θ_1}, i.e.,

$$\begin{aligned}
\mu_{\Delta_{1,i} \to x_{\theta_1}}^{(l)} &= \int \prod_{m=1}^{N_{\mathrm{RX}}} \mu_{g_{R_m} \to x_{\theta_i}}^{(l)}(x_{\theta_i}) \mu_{h_{D_i} \to x_{\theta_i}}^{(l)}(x_{\theta_i}) \Delta_{1,i}(x_{\theta_1}, x_{\theta_i}) dx_{\theta_i} \\
&= \int \prod_{m=1}^{N_{\mathrm{RX}}} \mu_{g_{R_m} \to x_{\theta_i}}^{(l)}(x_{\theta_i}) \Delta_{1,i}(x_{\theta_1}, x_{\theta_i}) dx_{\theta_i} \int \mu_{h_{D_i} \to x_{\theta_i}}^{(l)}(x_{\theta_i}) \Delta_{1,i}(x_{\theta_1}, x_{\theta_i}) dx_{\theta_i} \\
&\propto f_{\mathbf{R}}^{(l)}(x_{\theta_1}) N\left(x_{\theta_1}; m_{D_i, \Delta_{1,i} \to x_{\theta_1}}^{(l)}, (\sigma_{h_{D_i, \Delta_{1,i}} \to x_{\theta_1}}^{(l)})^2\right)
\end{aligned} \tag{29}$$

where

$$f_{\mathbf{R}}^{(l)}(x_{\theta_1}) \triangleq \prod_{m=1}^{N_{\mathrm{RX}}} \left(\frac{(1 - P_{\mathrm{VA}})}{R_{\max}} + \frac{P_{\mathrm{VA}}}{P_{\mathrm{v}}} \sum_{j=1}^{N_{\mathrm{RX}}} P_{\mathrm{v},j} N\left(x_{\theta_1}; m_{R_m, j, \Delta_{1,i} \to x_{\theta_1}}^{(l)}, \left(\sigma_{g_{R_m, j, \Delta_{1,i}} \to x_{\theta_1}}^{(l)}\right)^2\right) \right) \tag{30}$$

The former part $f_{\mathbf{R}}^{(l)}(x_{\theta_1})$ means the component attributed by measurements $\mathbf{R}$, the latter part in (29) represents the component attributed by D_i. Similar operation and expression is straightforward to coordinate y_{θ_i} in variable $\boldsymbol{\theta}_i$.

Thirdly, the message from G to $\boldsymbol{\theta}_1$ is

$$\mu_{G\to\boldsymbol{\theta}_1}^{(l)}(\boldsymbol{\theta}_1)=\prod_{m=1}^{N_{\mathrm{RX}}}\mu_{g_{R_m}\to\boldsymbol{\theta}_1}^{(l)}(\boldsymbol{\theta}_1)\propto\prod_{m=1}^{N_{\mathrm{RX}}}\left(\frac{(1-P_{\mathrm{VA}})}{R_{\max}}+\frac{P_{\mathrm{VA}}}{P_{\mathrm{v}}}\sum_{j=1}^{N_{\mathrm{RX}}}P_{\mathrm{v},j}N\left(\boldsymbol{\theta}_1;m_{g_{R_m,j}\to\boldsymbol{\theta}_1}^{(l)},(\sigma_{g_{R_m,j}\to\boldsymbol{\theta}_1}^{(l)})^2\right)\right) \tag{31}$$

Having all the messages transmitted from the neighboring factor nodes to the variable node $\boldsymbol{\theta}_1$, we are able to calculate the belief

$$b_{\boldsymbol{\theta}_1|\mathbf{R},\mathbf{D}}^{(l)}(\boldsymbol{\theta}_1)=\prod_{i=2}^{N_{\mathrm{RX}}}\mu_{\Delta_{1,i}\to\boldsymbol{\theta}_1}^{(l)}(\boldsymbol{\theta}_1)\mu_{G\to\boldsymbol{\theta}_1}^{(l)}(\boldsymbol{\theta}_1)\mu_{p_2\to\boldsymbol{\theta}_1}(\boldsymbol{\theta}_1)\mu_{h_{D_1}\to\boldsymbol{\theta}_1}^{(l)}(\boldsymbol{\theta}_1) \tag{32}$$

With the help of the prior information, substituting (29)-(31) and (43)-(44) into (31), and rearranging the results yields

$$b_{\boldsymbol{\theta}_1|\mathbf{R},\mathbf{D}}^{(l)}(\boldsymbol{\theta}_1)=b_{\boldsymbol{\theta}_1|\mathbf{R}}^{(l)}(\boldsymbol{\theta}_1)\mu_{h_{D_1}\to\boldsymbol{\theta}_1}^{(l)}(\boldsymbol{\theta}_1)\prod_{i=2}^{N_{\mathrm{RX}}}N\left(\boldsymbol{\theta}_1;m_{D_i,\Delta_{1,i}\to\boldsymbol{\theta}_1}^{(l)},(\sigma_{h_{D_i,\Delta_{1,i}}\to\boldsymbol{\theta}_1}^{(l)})^2\right) \tag{33}$$

where $b_{\boldsymbol{\theta}_1|\mathbf{R}}^{(l)}(\boldsymbol{\theta}_1)$ is defined as

$$b_{\boldsymbol{\theta}_1|\mathbf{R}}^{(l)}(\boldsymbol{\theta}_1)\triangleq\mu_{p_2\to\boldsymbol{\theta}_1}(\boldsymbol{\theta}_1)\mu_{G\to\boldsymbol{\theta}_1}^{(l)}(\boldsymbol{\theta}_1)\prod_{i=2}^{N_{\mathrm{RX}}}f_{\mathbf{R}}^{(l)}(x_{\theta_1}) \tag{34}$$

Obviously, the expression (32) cannot be directly employed as messages on factor graph due to the complicated structure in (33). Similar to the method to $b_{\boldsymbol{\varphi}|\mathbf{R}}^{(l)}(\boldsymbol{\varphi})$, we resort to approximate $b_{\boldsymbol{\theta}_1|\mathbf{R}}^{(l)}(\boldsymbol{\theta}_1)$ by Gaussian distributions via KLD minimization, which leads to

$$b_{\boldsymbol{\theta}_1|\mathbf{R}}^{(l)*}(\boldsymbol{\theta}_1)\propto N(\boldsymbol{\theta}_1;m_{\boldsymbol{\theta}_1}^{(l)},(\sigma_{\boldsymbol{\theta}_1}^{(l)})^2) \tag{35}$$

Substituting (34) into (32), we have

$$b_{\boldsymbol{\theta}_1|\mathbf{R},\mathbf{D}}^{(l)*}(\boldsymbol{\theta}_1)\propto \tag{36}$$

$$N\left(\boldsymbol{\theta}_1;(\sigma_{\boldsymbol{\theta}_1}^{(l)*})^2\left(\frac{m_{\boldsymbol{\theta}_1}^{l}}{(\sigma_{\boldsymbol{\theta}_1}^{(l)})^2}+\frac{m_{h_{D_1}\to\boldsymbol{\theta}_1}^{(l)}}{\left(\sigma_{h_{D_1}\to\boldsymbol{\theta}_1}^{(l)}\right)^2}+\sum_{i=2}^{N_{\mathrm{RX}}}\frac{m_{D_i,\Delta_{1,i}\to\boldsymbol{\theta}_1}^{(l)}}{\left(\sigma_{h_{D_i,\Delta_{1,i}\to\boldsymbol{\theta}_1}}^{(l)}\right)^2}\right),\left(\frac{1}{(\sigma_{\boldsymbol{\theta}_1}^{(l)})^2}+\frac{1}{\left(\sigma_{h_{D_1}\to\boldsymbol{\theta}_1}^{(l)}\right)^2}+\sum_{i=2}^{N_{\mathrm{RX}}}\frac{1}{\left(\sigma_{h_{D_i,\Delta_{1,i}\to\boldsymbol{\theta}_1}}^{(l)}\right)^2}\right)^{-1}\right)$$

where $(\sigma_{\boldsymbol{\theta}_1}^{(l)*})^2\triangleq\left(\frac{1}{(\sigma_{\boldsymbol{\theta}_1}^{(l)})^2}+\frac{1}{\left(\sigma_{h_{D_1}\to\boldsymbol{\theta}_1}^{(l)}\right)^2}+\sum_{i=2}^{N_{\mathrm{RX}}}\frac{1}{\left(\sigma_{h_{D_i,\Delta_{1,i}\to\boldsymbol{\theta}_1}}^{(l)}\right)^2}\right)^{-1}$.

The beliefs of target and receiver are sent to the connected factor node for next iteration. The above message updating procedure repeats until the convergence or the number of iterations reaches the maximum.

Finally, given the expressions of $b_{\boldsymbol{\varphi}|\mathbf{R}}^{(l)*}(x_\varphi),b_{\boldsymbol{\varphi}|\mathbf{R}}^{(l)*}(y_\varphi),b_{\boldsymbol{\theta}_1|\mathbf{R},\mathbf{D}}^{(l)*}\left(x_{\theta_1}\right)$ and $b_{\boldsymbol{\theta}_1|\mathbf{R},\mathbf{D}}^{(l)*}\left(y_{\theta_1}\right)$, we can calculate the positions of the target and receiver by MMSE estimators. The proposed algorithm is summarized in **Table 1**. Remark that we may receive more than N_{RX} range measurements in one time slot in practical scenarios. In this case, suitable amount of deterministic MPCs can be selected based on the method in [15] and the proposed algorithm is

still applicable. If the number of range measurements is less than three, we can drop the measurements and wait for the next time slot.

Table 1. The Proposed Passive Localization Algorithm

1)	Initialization: Set the target and receiver's initial position estimates $\hat{\boldsymbol{\varphi}} \triangleq [x_{\varphi}\ y_{\varphi}]^T$ and $\boldsymbol{\theta}_1 \triangleq [x_{\theta_1}\ y_{\theta_1}]^T$ according to the prior distributions $p_1(x_{\varphi}) \propto N\left(x_{\varphi}; x_{\bar{\varphi}}, (\sigma_{x_{\varphi}}^{(0)})^2\right),\ p_1(y_{\varphi}) \propto N\left(y_{\varphi}; y_{\bar{\varphi}}, (\sigma_{y_{\varphi}}^{(0)})^2\right);$ $p_2(x_{\theta_1}) \propto N\left(x_{\theta_1}; x_{\bar{\theta}_1}, (\sigma_{x_{\theta_1}}^{(0)})^2\right),\ p_2(y_{\theta_1}) \propto N\left(y_{\theta_1}; y_{\bar{\theta}_1}, (\sigma_{x_{\theta_1}}^{(0)})^2\right);$

2)	The positions of virtual receivers $\boldsymbol{\theta}_i, i \in \{2,..., N_{\mathrm{RX}}\}$ are initialized according to indicator $\Delta_{1,i}(\boldsymbol{\theta}_1, \boldsymbol{\theta}_{i\setminus 1})$
	For $l = 1$ to N_{iter} do
	Calculate the messages from factor $\Delta_{1,i}$ to virtual receiver $\boldsymbol{\theta}_i$ by (18) and (19);
	Calculate the messages from factor G to target $\boldsymbol{\varphi}$ by (20);
	Calculate the beliefs of the target position by (21) and minimize the KLD to obtain (26);
	Calculate the messages from factor G to $\boldsymbol{\theta}_i$ by (27), and the messages from factor H to $\boldsymbol{\theta}_i$ by (43) and (44);
	Calculate the messages from factor $\Delta_{1,i}$ to $\boldsymbol{\theta}_1$ by (29) and from factor G to $\boldsymbol{\theta}_1$ by (31);
	Calculate the belief $b_{\boldsymbol{\theta}_1\mid\mathbf{R}}^{(l)}(\boldsymbol{\theta}_1)$ by (34) and minimize the KLD to obtain (35);
	Calculate the beliefs of receiver position by (36);
	Update the means and variances of the virtual receivers' positions using the indicator function $\Delta_{1,i}(\boldsymbol{\theta}_1, \boldsymbol{\theta}_{i\setminus 1}), i \in \{2,..., N_{\mathrm{RX}}\}$;
	End For;

3)	Estimate positions of target and receiver using MMSE estimator.

5. Simulation Results

The proposed algorithm is evaluated by Monte Carlo simulations, with parameters shown in **Table 2.** Considering a room with known layout. Positions of the target and receiver are initialized based on standard deviations $\sigma_{\boldsymbol{\varphi}}$ and $\sigma_{\boldsymbol{\theta}_1}$. The standard deviations of the range measurement noise σ_{R_m} and σ_{D_i} of each link are uniformly distributed. For the proposed algorithm, N_{KLD} samples and M_{KLD} iterations are employed to minimize the KLD in (25).

Table 2. Simulation Parameters

Parameter	Note	Value	Parameter	Note	Value
L × W	Room dimensions	$10m \times 8m$	$[x_{\theta_1}\ y_{\theta_1}]^T$	Receiver location	$[7m\ 5m]^T$
σ_{R_m}	Ranging noise R_m	$0.1m \sim 0.3m$	$[x_\varphi\ y_\varphi]^T$	Target location	$[2m\ 7m]^T$
σ_{D_i}	Ranging noise D_i	$0 \sim 0.2m$	N_{RX}	Deterministic MPCs	$3 \le N_{\mathrm{RX}} \le 5$
$\sigma_{\boldsymbol{\theta}_i}$	Prior standard deviations	0.5m	M	Number of iterations	20
$\sigma_{\boldsymbol{\varphi}}$	Prior standard deviations	1m	N_{AMAP}	Fine girds in AMAP	50×50
$P_{\mathrm{v},p}$	LOS	0.8	N_{KLD}	Samples to min. KLD	100
	Single reflections	0.5			
P_{VA}	R_m in **R**	0.9	M_{KLD}	Iterations	10

The cumulative distribution function (CDF) of the target positioning error is illustrated in **Fig. 4**. For comparison purpose, particle-based algorithm and approximated maximum *a posteriori* probability (AMAP) algorithm, are also evaluated. Particle-based algorithm uses particles to represent messages, which avoid the Taylor expansion of nonlinear function and Gaussian approximation of messages employed in the proposed algorithm, at the cost of huge computational complexity which is proportional to the number of particles used [16]. In AMAP method, the position estimates of target and receiver instead of the distribution functions are employed in the estimation, which means the uncertainties of positions are ignored in localization. It is seen that all the three algorithms improve the prior localization accuracy. Increasing the number of particles N_p will improve the localization accuracy of the target. However, the performance gain becomes negligible with large N_p. The proposed algorithm outperforms the AMAP method and the particle-based algorithm with $N_p = 1000$, and performs very close to the latter with $N_p = 6000$.

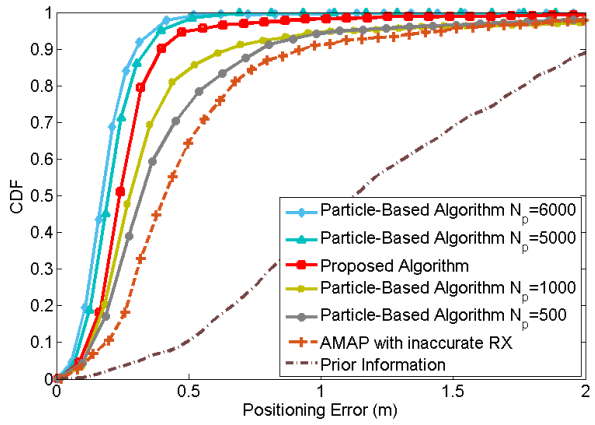

Fig. 4. CDF of the positioning error of the target

Similar CDF results can be observed in **Fig. 5**, which shows the receiver's positioning error.

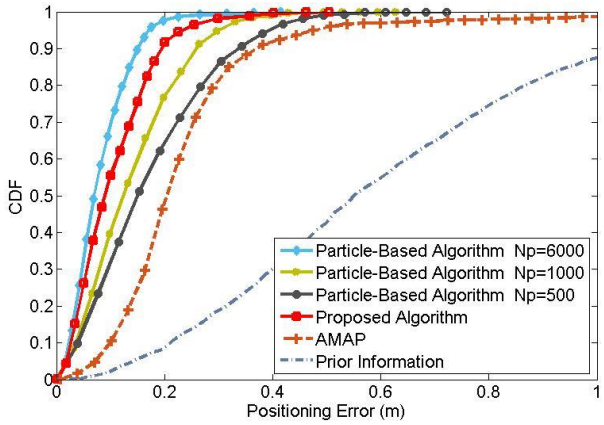

Fig. 5. CDF of the positioning error of the receiver

The mean squared error (MSE) performance of the proposed algorithm, AMAP and particle-based algorithm versus the number of iterations are compared in **Fig. 6**. We can observe that particle-based algorithm converges very fast at the cost of computational complexity. The convergence speed of the proposed algorithm is faster than that of the AMAP estimator.

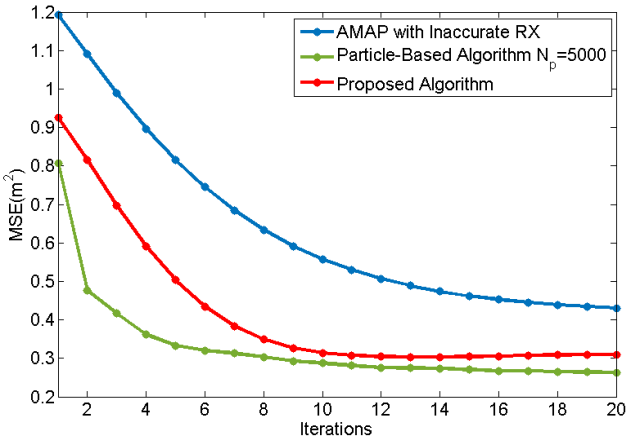

Fig. 6. MSE of target positioning error versus the number of iterations

The numbers of received deterministic MPCs and clutters are random variables that are determined by the parameters in **Table 2.** To evaluate the impact of the two signals, localization performance with different numbers of deterministic MPCs and clutters are evaluated in **Fig. 7**. We can observe that the appearance of clutters will significantly degrade the performance. Moreover, when the number of received deterministic MPCs increases, the localization accuracy can be improved.

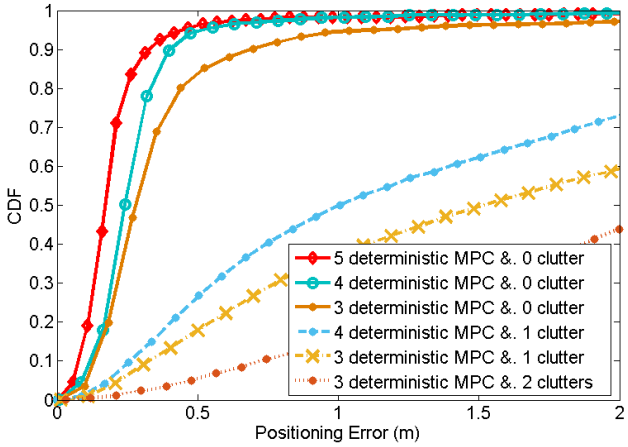

Fig. 7. Positioning error of the target with different numbers of deterministic MPCs and clutters

One of the challenges in indoor wideband localization is the data association, i.e., to associate different paths with TOA observations. However, this model in (3) intrinsically allows the same R_m to be associated with different virtual receivers, which leads to multiple local maxima in the likelihood function. This problem can be alleviated by including the constraint of target's prior distribution. We evaluate the impact of the employed model with different prior distributions in **Fig. 8**. It can be observed that the performance gap between ideal data association and the employed model which does not perform data association are small. When the standard deviation of prior distribution increases, the posterior distribution may contain more local maxima which degrade the localization performance.

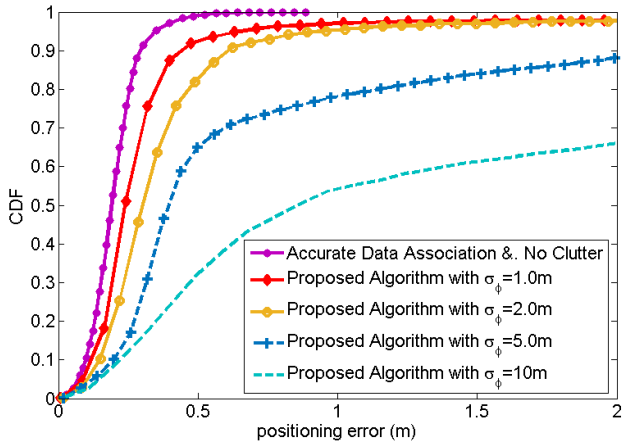

Fig. 8. CDF of the positioning error of the target with different prior position information

In practice, receiver may not be able to perfectly know the statistics of the multipath channel, which means the values of P_{VA} and $P_{\mathrm{v},p}$ may be different from the real values. To evaluate the robustness of the proposed algorithm with inaccurate channel information, we compare the localization accuracy of the proposed algorithm by varying the value of P_{VA} in the likelihood function in **Fig. 9**. This scenario means that the receiver may not have the perfect knowledge whether a range measurement belongs to deterministic MPCs. It can be seen that the best

localization accuracy is obtained when the value of P_{VA} matches the real value. We can observe that when P_{VA} employed in the likelihood function is close to the real value, e.g., $P_{\mathrm{VA}} = 0.95, 0.85$, the performance loss is negligible. However, when significant mismatch happens, e.g., $P_{\mathrm{VA}} = 0.1$ is employed, large performance degradation can be observed due to the increased possibility that mapping the deterministic MPC as clutters and the clutters vice versa.

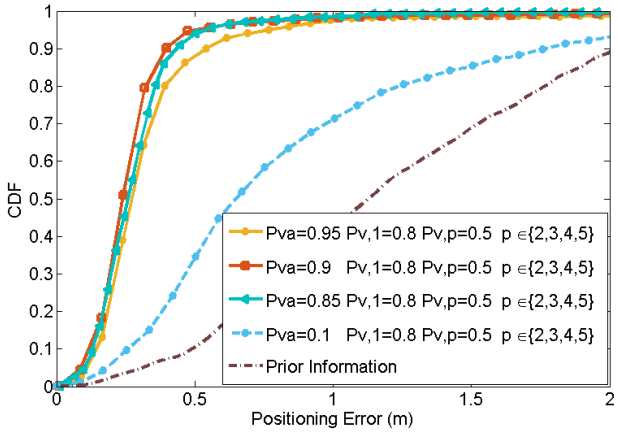

Fig. 9. CDF of the positioning error of the target with different parameters P_{VA}

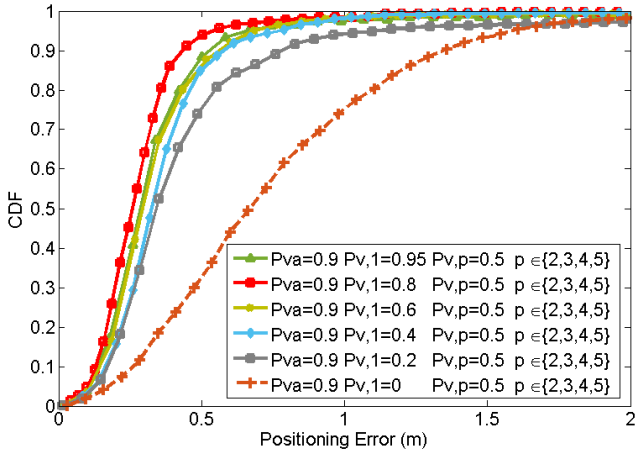

Fig. 10. CDF of the positioning error of the target with different parameters $P_{\mathrm{v},p}$

The robustness of the proposed algorithm to the value of $P_{\mathrm{v},p}$, which represents the probability that the deterministic MPC is a LOS component or a single reflection, is also evaluated in **Fig. 10**. Note that although $P_{\mathrm{v},p} = 0.5 \;\; p \in \{2,3,4,5\}$ is illustrated, since $P_{\mathrm{v},p}$ will be normalized by P_{v} in (3), the different value of $P_{\mathrm{v},1}$ will lead to the variation of $P_{\mathrm{v},p} / P_{\mathrm{v}}$. As we expected, it is seen that the best localization performance is obtained when the parameter $P_{\mathrm{v},1}$ in the likelihood function matches the one used in the model to generate LOS component. However, the performance gaps by adopting different values of $P_{\mathrm{v},1}$ are small, which

demonstrates that the performance is not sensitive to the value of $P_{v,1}$. The reason for this phenomenon is that the local maxima in (3) determined by different values of $P_{v,1}$ has an exponential decay due to the Gaussian prior. The true maxima constrained by the prior will have higher weight than other local maxima and the belief of target will have a smaller variance than prior information after minimizing KLD. An exception is that $P_{v,1}=0$, which results in a very poor performance. This is due to the fact that, the algorithm has to adjust the mapping mode to satisfy the assumption that there is no measurement coming from a certain receiver or virtual receiver, which significantly decreases the localization performance.

Table 3. Computational Complexity of Three Algorithms

Algorithm	Computational complexity	Values
AMAP Alg.	$O(N_{AMP}N_{RX}^2M)$	$N_{AMAP}=2500$
Proposed Alg.	$O(N_{KLD}M_{KLD}N_{RX}^2M)$	$N_{KLD}M_{KLD}=1000$
Particle-Based Alg.	$O(N_pN_{RX}^2M)$	N_{RX} and M are small but N_p is large

Table 3 illustrates the computational complexities of AMAP, particle-based algorithm and the proposed algorithm. Although AMAP does not need to minimize KLD to represent belief of variable, its computational complexity is still high due to the fine grids method employed. The computational complexity of particle-based algorithm depends on the number of particles N_p, which is very large in order to obtain an acceptable performance. For the proposed algorithm, simulation results show that the product $M_{KLD}N_{KLD}$ is much smaller than N_p to obtain the similar localization accuracy, which makes the proposed algorithm attractive in practice.

6. Conclusion

In this paper, we studied an indoor passive localization of the target equipped with RFID device in UWB wireless network. Due to the fine resolution of UWB signal, deterministic multipath components (MPCs) were used to locate the target by one transmitter and one inaccurate receiver. However, due to the mixed distribution in the likelihood function and the nonlinear terms included, it was intractable to derive the messages on factor graph using belief propagation directly. We employed two methods to solve this problem. First, the nonlinear terms were linearized by Taylor expansion around the previous position estimation. Second, intractable message was approximated by Gaussian distribution via minimizing the Kullback-Leibler divergence (KLD) between them. Since only the means and variances have to be updated, the proposed algorithm significantly reduced the computational complexity. Simulation results showed that the proposed algorithm outperformed the approximated maximum a posteriori probability (AMAP) algorithm and the particle-based algorithm when the number of particles is not very large. The impact of critical parameters of the proposed algorithm and the robustness to the statistics of multipath channels were also evaluated.

Appendix A

In this appendix, we derive messages from $g_{R_m}(\boldsymbol{\theta},\boldsymbol{\varphi})$ in $G(\boldsymbol{\theta},\boldsymbol{\varphi})$ to $\varphi=\left(x_\varphi, y_\varphi\right)$.

$$\begin{aligned}\mu^{(l)}_{g_{R_m}\to x_\varphi}(x_\varphi) \propto \int\cdots\int p(R_m \mid x_\varphi, y_\varphi, x_{\theta_1}, y_{\theta_1}, \cdots x_{\boldsymbol{\theta}_{N_{\mathrm{RX}}}}, y_{\boldsymbol{\theta}_{N_{\mathrm{RX}}}}) \\ \cdot\mu^{(l-1)}_{y_\varphi\to g_{R_m}}(y_\varphi)\mu^{(l-1)}_{x_{\theta_1}\to g_{R_m}}(x_{\theta_1})\mu^{(l-1)}_{y_{\theta_1}\to g_{R_m}}(y_{\theta_1})\cdots dy_\varphi d\boldsymbol{\theta}\end{aligned} \tag{37}$$

The expressions of messages $\mu^{(l)}_{g_{R_m}\to y_\varphi}(y_\varphi)$ can be calculated in a similar way. We remark that only the expressions of messages to x coordinate are given in the following context for brevity.

Using belief propagation algorithm in this indoor passive scenario, we will find the message in $\mu^{(l)}_{g_{R_m}\to x_\varphi}(x_\varphi)$ and $\mu^{(l)}_{g_{R_m}\to x_{\theta_i}}(x_{\theta_i})$ are intractable due to the nonlinear term in the likelihood function. In order to obtain the closed-form expression, we use Taylor series expansion to the latter part of (3) and (7) [17].

For factor G with measurements $R_m, m\in\{1,...,N_{\mathrm{RX}}\}$, unlike the sub-factor node $h_{D_i}(\boldsymbol{\theta}_i)$ in H that connects to only one variable $\boldsymbol{\theta}_i$, each sub-factor $g_{R_m}(\boldsymbol{\theta},\boldsymbol{\varphi})$ in G connects to all the variables $\boldsymbol{\theta}_i$, $i\in\{1,...,N_{\mathrm{RX}}\}$. For the messages from $g_{R_m}(\boldsymbol{\theta},\boldsymbol{\varphi})$ to $\boldsymbol{\varphi}$, the former part in (3) is unchanged after the integration. The latter part in (3) turns to be a Gaussian distribution after linearization, i.e.

$$N(\boldsymbol{\varphi}; m^{(l)}_{g_{R_m,\boldsymbol{\theta}_j}\to\boldsymbol{\varphi}}, (\sigma^{(l)}_{g_{R_m,\boldsymbol{\theta}_j}\to\boldsymbol{\varphi}})^2) = \tag{38}$$

$$N\left(\boldsymbol{\varphi}; \left(\frac{\left(R_m-\hat{d}^{(l-1)}_{\phi-\boldsymbol{\varphi}}\right)}{\hat{d}^{(l-1)}_{\boldsymbol{\varphi}-\boldsymbol{\theta}_j}}\left(\boldsymbol{\varphi}^{(l-1)}-\boldsymbol{\theta}^{(l-1)}_j\right)+\bar{\boldsymbol{\theta}}_j\right)\frac{\sigma^2_{R_j}}{2\sigma^2_{R_j}+\left(\sigma^{(l-1)}_{\boldsymbol{\theta}_j}\right)^2}+\frac{\left(R_m-\hat{d}^{(l-1)}_{\boldsymbol{\varphi}-\boldsymbol{\theta}_j}\right)}{\hat{d}^{(l-1)}_{\phi-\boldsymbol{\varphi}}}\frac{\left(\sigma^2_{R_j}+\left(\sigma^{(l-1)}_{\boldsymbol{\theta}_j}\right)^2\right)}{2\sigma^2_{R_j}+\left(\sigma^{(l-1)}_{\boldsymbol{\theta}_j}\right)^2}\boldsymbol{\varphi}^{(l-1)}, \frac{\sigma^2_{R_j}\left(\sigma^2_{R_j}+\left(\sigma^{(l-1)}_{\boldsymbol{\theta}_j}\right)^2\right)}{2\sigma^2_{R_j}+\left(\sigma^{(l-1)}_{\boldsymbol{\theta}_j}\right)^2}\right)$$

where $\hat{\boldsymbol{\varphi}}^{(l-1)} \triangleq [\hat{x}^{(l-1)}_\varphi \ \hat{y}^{(l-1)}_\varphi]^T$ and $\hat{\boldsymbol{\theta}}^{(l-1)}_j \triangleq [\hat{x}^{(l-1)}_{\theta_j} \ \hat{y}^{(l-1)}_{\theta_j}]^T$ are the position estimates in the previous iteration. $\hat{d}^{(l-1)}_{\phi-\boldsymbol{\varphi}} \triangleq \sqrt{\left(\hat{x}^{(l-1)}_\varphi\right)^2+\left(\hat{y}^{(l-1)}_\varphi\right)^2}$, $\hat{d}^{(l-1)}_{\boldsymbol{\varphi}-\boldsymbol{\theta}_j} \triangleq \sqrt{\left(\hat{x}^{(l-1)}_\varphi-\hat{x}^{(l-1)}_{\theta_j}\right)^2+\left(\hat{y}^{(l-1)}_\varphi-\hat{y}^{(l-1)}_{\theta_j}\right)^2}$ are the estimated Euclidean distances.

Therefore, the message $\mu^{(l)}_{g_{R_m}\to\boldsymbol{\varphi}}(\boldsymbol{\varphi})$ can be expressed as

$$\mu^{(l)}_{g_{R_m}\to\boldsymbol{\varphi}}(\boldsymbol{\varphi}) \propto \frac{(1-P_{\mathrm{VA}})}{R_{\max}}+\frac{P_{\mathrm{VA}}}{P_{\mathrm{v}}}\sum_{j=1}^{N_{\mathrm{RX}}}P_{\mathrm{v},j}N(\boldsymbol{\varphi}; m^{(l)}_{g_{R_m,\boldsymbol{\theta}_j}\to\boldsymbol{\varphi}}, (\sigma^{(l)}_{g_{R_m,\boldsymbol{\theta}_j}\to\boldsymbol{\varphi}})^2) \tag{39}$$

Appendix B

In this appendix, we derive messages from g_{R_m} to $\boldsymbol{\theta}_i$ and messages from h_{D_i} to $\boldsymbol{\theta}_i$.

$$\begin{aligned}\mu^{(l)}_{g_{R_m}\to x_{\theta_i}}(x_{\theta_i}) \propto \int\cdots\int p(R_m \mid x_\varphi, y_\varphi, x_{\theta_1}, y_{\theta_1}, \cdots x_{\boldsymbol{\theta}_{N_{\mathrm{RX}}}}, y_{\boldsymbol{\theta}_{N_{\mathrm{RX}}}}) \\ \cdot\mu^{(l-1)}_{x_\varphi\to g_{R_m}}(x_\varphi)\mu^{(l-1)}_{y_\varphi\to g_{R_m}}(y_\varphi)\mu^{(l-1)}_{y_{\theta_1}\to g_{R_m}}(y_{\theta_1})\cdots dx_\varphi dy_\varphi d\boldsymbol{\theta}\setminus x_{\theta_i}\end{aligned} \tag{40}$$

Similarly to Appendix A, we show the expressions of messages to x coordinate only.

The former part in $p(R_m \mid x_\varphi, y_\varphi, x_{\theta_1}, y_{\theta_1}, \cdots x_{\boldsymbol{\theta}_{N_{\mathrm{RX}}}}, y_{\boldsymbol{\theta}_{N_{\mathrm{RX}}}})$ remains unchanged and each component in the latter part turns to be a Gaussian distribution after appropriate normalization, i.e.

$$N(\boldsymbol{\theta}_i; m^{(l)}_{g_{R_m,j}\to\boldsymbol{\theta}_i}, (\sigma^{(l)}_{g_{R_m,j}\to\boldsymbol{\theta}_i})^2) = \tag{41}$$

$$N\left(\boldsymbol{\theta}_i; \frac{\left(R_m - \hat{d}^{(l-1)}_{\boldsymbol{\varphi}-\boldsymbol{\theta}_i}\right)}{\hat{d}^{(l-1)}_{\phi-\boldsymbol{\varphi}}} \frac{\left(\sigma^{(l-1)}_{\boldsymbol{\varphi}}\right)^2}{\sigma^2_{R_j} + \left(\sigma^{(l-1)}_{\boldsymbol{\varphi}}\right)^2} \hat{\boldsymbol{\varphi}}^{(l-1)} + \frac{\left(R_m - \hat{d}^{(l-1)}_{\phi-\boldsymbol{\varphi}}\right)}{\hat{d}^{(l-1)}_{\boldsymbol{\varphi}-\boldsymbol{\theta}_i}} \left(\boldsymbol{\theta}^{(l-1)}_j - \hat{\boldsymbol{\varphi}}^{(l-1)}\right) + \frac{\sigma^2_{R_j}\bar{\boldsymbol{\varphi}}}{\sigma^2_{R_j} + \left(\sigma^{(l-1)}_{\boldsymbol{\varphi}}\right)^2}, \frac{\sigma^2_{R_j}\left(2\left(\sigma^{(l-1)}_{\boldsymbol{\varphi}}\right)^2 + \sigma^2_{R_j}\right)}{\left(\sigma^{(l-1)}_{\boldsymbol{\varphi}}\right)^2 + \sigma^2_{R_j}}\right)$$

where $\hat{\boldsymbol{\varphi}}^{(l-1)} \triangleq [\hat{x}^{(l-1)}_\varphi \ \hat{y}^{(l-1)}_\varphi]^T$ and $\hat{\boldsymbol{\theta}}^{(l-1)}_j \triangleq [\hat{x}^{(l-1)}_{\theta_j} \ \hat{y}^{(l-1)}_{\theta_j}]^T$ are the position estimates in the previous iteration.

So the message from $g_{R_m}(\boldsymbol{\theta}, \boldsymbol{\varphi})$ to $\boldsymbol{\theta}_i$ can be expressed as a mixture marginal distribution of variable $\boldsymbol{\theta}_i$, i.e.

$$\mu^{(l)}_{g_{R_m}\to\boldsymbol{\theta}_i}(\boldsymbol{\theta}_i) \propto \frac{(1-P_{\mathrm{VA}})}{R_{\max}} + \frac{P_{\mathrm{VA}}}{P_{\mathrm{v}}} \sum_{j=1}^{N_{\mathrm{RX}}} P_{\mathrm{v},j} N(\boldsymbol{\theta}_i; m^{(l)}_{g_{R_m,j}\to\boldsymbol{\theta}_i}, (\sigma^{(l)}_{g_{R_m,j}\to\boldsymbol{\theta}_i})^2) \tag{42}$$

Besides, factor H with measurements $D_i, i \in \{1,...,N_{\mathrm{RX}}\}$ also has messages to $\boldsymbol{\theta}_i$, using Taylor expansion of (3), messages from h_{D_i} to $\boldsymbol{\theta}_i \triangleq [x_{\theta_i} \ y_{\theta_i}]^T$ are

$$\mu^{(l)}_{h_{D_i}\to x_{\theta_i}} = \int p(D_i \mid \boldsymbol{\theta}_i) \mu^{(l-1)}_{y_{\theta_i}\to h_{D_i}}(y_{\theta_i}) dy_{\theta_i} \propto N\left(x_{\theta_i}; m^{(l)}_{h_{D_i}\to x_{\theta_i}}, (\sigma^{(l)}_{h_{D_i}\to x_{\theta_i}})^2\right) \tag{43}$$

$$\mu^{(l)}_{h_{D_i}\to y_{\theta_i}} = \int p(D_i \mid \boldsymbol{\theta}_i) \mu^{(l-1)}_{x_{\theta_i}\to h_{D_i}}(x_{\theta_i}) dx_{\theta_i} \propto N\left(y_{\theta_i}; m^{(l)}_{h_{D_i}\to y_{\theta_i}}, (\sigma^{(l)}_{h_{D_i}\to y_{\theta_i}})^2\right) \tag{44}$$

with means $m^{(l)}_{h_{D_i}\to x_{\theta_i}} = D_i \hat{x}^{(l-1)}_{\theta_i} / \hat{d}^{(l-1)}_{\phi-\boldsymbol{\theta}_i}, m^{(l)}_{h_{D_i}\to y_{\theta_i}} = D_i \hat{y}^{(l-1)}_{\theta_i} / \hat{d}^{(l-1)}_{\phi-\boldsymbol{\theta}_i}$ and variances $(\sigma^{(l)}_{h_{D_i}\to x_{\theta_i}})^2 = (\sigma^{(l)}_{h_{D_i}\to y_{\theta_i}})^2 = \sigma^2_{D_i}$. $\hat{d}^{(l-1)}_{\phi-\boldsymbol{\theta}_i} \triangleq \sqrt{\left(\hat{x}^{(l-1)}_{\theta_i}\right)^2 + \left(\hat{y}^{(l-1)}_{\theta_i}\right)^2}$, $i \in \{1,...,N_{\mathrm{RX}}\}$ is the estimated Euclidean distance between transmitter and $i-th$ receiver.

References

[1] H. H. Bi and D. Lin, "RFID-enabled discovery of supply networks," *IEEE Transactions on Engineering Management*, vol. 56, no. 1, pp. 129-141, 2009. Article (CrossRef Link)

[2] B. Gedik and L. Liu, "Mobieyes: A distributed location monitoring service using moving location queries," *IEEE Transactions on Mobile Computing*, vol. 5, no. 10, pp. 1384-1402, 2006. Article (CrossRef Link)

[3] S. Gezici, Z. Tian and G. B. Giannakis, "Localization via ultra-wideband radios: a look at positioning aspects for future sensor networks," *IEEE Signal Processing Magazine*, vol. 22, no. 4, pp. 70-84, 2005. Article (CrossRef Link)

[4] N. Patwari and J. Wilson, "RF sensor networks for device-free localization: Measurements, models, and algorithms," in *Proc. of the IEEE*, vol. 98, no. 11, pp. 1961-1973, 2010. Article (CrossRef Link)

[5] C. K. Seow and S. Y. Tan, "Non-line-of-sight localization in multipath environments," *IEEE Transactions on Mobile Computing*, vol. 7, no. 5, pp. 647-660, 2008. Article (CrossRef Link)

[6] B. Friedlander, "A passive localization algorithm and its accuracy analysis," *IEEE Journal of Oceanic Engineering*, vol. 12, no. 1, pp. 234-245, 1987. Article (CrossRef Link)

[7] K. Witrisal, E. Leitinger and P. Meissner, "Cognitive radar for the localization of RFID transponders in dense multipath environments," in *Proc. of IEEE Radar Conference (RADAR)*, pp. 1-6, 2013. Article (CrossRef Link)

[8] N. Decarli, F. Guidi and D. Dardari, "A novel joint RFID and radar sensor network for passive localization: Design and performance bounds," *IEEE Journal of Selected Topics in Signal Processing*, vol. 8, no. 1, pp. 80-95, 2014. Article (CrossRef Link)
[9] F. R. Kschischang, B. J. Frey and H.-A Loeliger, "Factor graphs and the sum-product algorithm," *IEEE Transactions on Information Theory*, vol. 47, no. 2, pp. 498-519, 2001. Article (CrossRef Link)
[10] J. Shen, F. A. Molisch and J. Salmi, "Accurate passive location estimation using TOA measurements," *IEEE Transactions on Wireless Communications*, vol. 11, no. 6, pp. 2182-2192, 2012. Article (CrossRef Link)
[11] W. Yuan, S. Ma and C. P. Chen, "TOA-Based Passive Localization in Quasi-Synchronous Networks," *IEEE Communications Letters*, vol. 18, no. 4, pp. 592-595, 2014. Article (CrossRef Link)
[12] S. Yuan, and M. Z. Win, "On the use of multipath geometry for wideband cooperative localization," in *Proc. of IEEE GLOBECOM on Global Telecommunications Conference*, pp. 1-6, 2009. Article (CrossRef Link)
[13] E. Leitinger, P. Meissner and M. Frohle, "Performance bounds for multipath-assisted indoor localization on backscatter channels," in *Proc. of Radar Conference (RADAR)*, pp. 70-75, 2014. Article (CrossRef Link)
[14] T. M. Cover and J. A. Thomas, *Elements of information theory*, 2nd Edition, Wiley, New York, 2009. Article (CrossRef Link)
[15] P. Meissner and K. Witrisal, "Multipath-assisted single-anchor indoor localization in an office environment," in *Proc. of 19th International Conference on Systems, Signals and Image Processing*(IWSSIP), pp. 22-25, 2012.
[16] D. M. Petar, K. H. Jayesh and J. Zhang, "Particle filtering," *IEEE Signal Processing Magazine*, no. 20, pp. 19-38, 2003. Article (CrossRef Link)
[17] N. Wu, B. Li, H. Wang, "Distributed cooperative localization based on Gaussian message passing on factor graph in wireless networks," *Science China Information Sciences*, no. 58, pp. 1-15, 2015. Article (CrossRef Link)

Ganlin Hao received the B.S. degree from Huazhong University of Science and Technology, Wuhan, China, in 2013. He is currently working toward his Master degree at School of Information and Electronics, Beijing Institute of Technology. His current research interests include the indoor localization and distributed signal processing.

Nan Wu received his Ph.D degree from Beijing Institute of Technology (BIT), Beijing, China in 2011. He is currently an Associate Professor at the School of Information and Electronics, BIT. From Nov. 2008 to Nov. 2009, he was a visiting Ph.D student with the Department of Electrical Engineering, Pennsylvania State University, USA. He is the recipient of National Excellent Doctoral Dissertation Award by MOE of China in 2013. His research interests include signal processing in wireless communications. He serves as editorial board members for International Journal of Electronics and Communications and KSII Transactions on Internet and Information Systems.

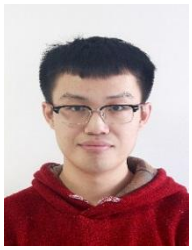

Yifeng Xiong received the B.S. degree from Beijing Institute of Technology (BIT), Beijing, China in 2015. He is currently working toward his Master degree at the School of Information and Electronics, BIT. His current research interests include cooperative localization and distributive signal processing.

Hua Wang received his Ph.D degree from Beijing Institute of Technology (BIT), Beijing, China, in 1999. He is now a Professor with School of Information and Electronics, BIT. From Feb. 2009 to Jan. 2010, he was a visiting scholar with the Department of Electrical Engineering, Arizona State University, USA. His research interests are in the fields of communication theory and signal processing.

Jingming Kuang received the Ph.D degree in Electrical Engineering from Technical University of Berlin, Berlin, Germany, in 1988. He has been a Professor with the School of Information and Electronics, Beijing Institute of Technology (BIT) since 1989. He is the founder of BIT-Ericsson Research Center of Digital Communications, which was built in 1999. From Aug. 1993 to Aug. 2007, he has been the vice-president and the president of Beijing Institute of Technology. His research interests include theory and techniques of wireless communication and digital signal processing. He published two books, more than 100 papers, and held several patents. Prof. Kuang is a member of subject evaluation of National Department Degree Council and the vice director of communication branch of Chinese Electronic Society. He is the recipient of Excellent Returnee from Abroad, Outstanding Scholar with Extraordinary Achievements, and Outstanding Scholar of National Defense Department.